HHS Public Access

Author manuscript

Nanomedicine. Author manuscript; available in PMC 2017 April 01.

Published in final edited form as:

Nanomedicine. 2016 April ; 12(3): 811–821. doi:10.1016/j.nano.2015.10.004.

Nanoparticle Facilitated Inhalational Delivery of Erythropoietin Receptor cDNA Protects Against Hyperoxic Lung Injury

Priya Ravikumar, PhD[1,4,§], **Jyothi U. Menon, PhD**[2,§], **Primana Punnakitikashem, MSc**[2], **Dipendra Gyawali, MSc**[1], **Osamu Togao, MD, PhD**[3], **Masaya Takahashi, PhD**[3], **Jianning Zhang, MD**[1], **Jianfeng Ye, MD**[1,4], **Orson W. Moe, MD**[1,4], **Kytai T. Nguyen, PhD**[2,*], and **Connie C.W. Hsia, MD**[1,*]

[1]Department of Internal Medicine, University of Texas Southwestern Medical Center, Dallas, TX

[2]Department of Bioengineering, University of Texas at Arlington, Arlington, TX

[3]Department of Radiology and Advanced Imaging Research Center, University of Texas Southwestern Medical Center, Dallas, TX

[4]Charles and Jane Pak Center for Mineral Metabolism and Clinical Research, University of Texas Southwestern Medical Center, Dallas, TX

Abstract

Our goals were to develop and establish nanoparticle (NP)-facilitated inhalational gene delivery, and to validate its biomedical application by testing the hypothesis that targeted upregulation of pulmonary erythropoietin receptor (EpoR) expression protects against lung injury. Poly-lactic-co-glycolic acid (PLGA) NPs encapsulating various tracers were characterized and nebulizated into rat lungs. Widespread NP uptake and distribution within alveolar cells were visualized by magnetic resonance imaging, and fluorescent and electron microscopy. Inhalation of nebulized NPs bearing EpoR cDNA upregulated pulmonary EpoR expression and downstream signal transduction (ERK1/2 and STAT5 phosphorylation) in rats for up to 21 days, and attenuated hyperoxia-induced damage in lung tissue based on apoptosis, oxidative damage of DNA, protein and lipid, tissue edema, and alveolar morphology compared to vector-treated control animals. These results establish the feasibility and therapeutic efficacy of NP-facilitated cDNA delivery to the lung, and demonstrate that targeted pulmonary EpoR upregulation mitigates acute oxidative lung damage.

[*]Corresponding Authors: Connie C.W. Hsia, M.D., Pulmonary and Critical Care Medicine, Department of Internal Medicine, University of Texas Southwestern Medical Center, 5323 Harry Hines Blvd., Dallas, TX 75390-9034, TEL: 214-648-3426; FAX: 214-648-8027, Connie.Hsia@utsouthwestern.edu. Kytai T. Nguyen, Ph.D., Dept. of Bioengineering, University of Texas at Arlington, 500 UTA Blvd. ERB-241, TEL: 817-272-2540; FAX: 817-272-2251, Knguyen@uta.edu.

[§]These authors contributed equally to this work.

Present address of Dr. Osamu Togao: Department of Molecular Imaging and Diagnosis, Kyushu University, Fukuoka, Japan.

The authors have no conflict of interest to declare.

The content is solely the responsibility of the authors and does not necessarily represent the official views of the National Institutes of Health.

The authors have no disclosures and no conflicts of interest to declare.

Graphical Abstract

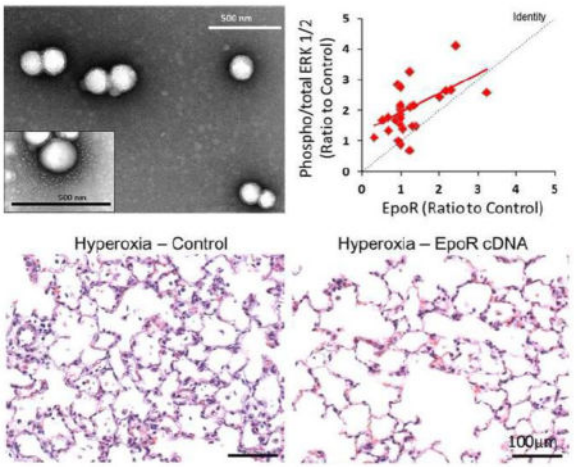

To test the hypothesis that targeted upregulation of pulmonary erythropoietin (Epo) signaling via its receptor (EpoR) protects against lung injury, we encapsulated EpoR cDNA within poly-lacticco-glycolic acid (PLGA) nanoparticles (NPs), and optimized nebulization into rat lungs. We observed sustained increases in EpoR protein expression and activation of downstream signal transduction – phospho/total ERK1/2 (*shown above*) and STAT5 – peaking at 10 days and persisting up to 21 days, associated with attenuation of hyperoxia-induced lung injury. These results establish the feasibility and efficacy of a novel non-invasive approach of nanoparticle-facilitated gene therapy for acute lung injury.

Keywords

Poly-lactic-co-glycolic acid nanoparticles; aerosol nebulization; oxidative stress damage; gene therapy; cytoprotection; hyperoxia

Introduction

Acute lung injury resulting from inflammation, smoke inhalation, or other insults leading to adult respiratory distress syndrome is an important clinical problem with high morbidity and mortality. (1) Current management focuses on ventilatory support and treatment of the underlying cause. Pharmacologic approaches using glucocorticoids, exogenous surfactant, inhaled nitric oxide, and N-acetylcysteine, among many others, have not reduced mortality. (1) There remains a need for novel therapy designed specifically to protect lung tissue against the inciting insults and facilitate repair. Paracrine/autocrine erythropoietin (Epo) signaling via its receptor (EpoR) has been shown to counteract inflammatory injury by suppressing apoptosis, (2) promoting angiogenesis, (3–5) and offering trophic support for repair and remodeling. (2, 6–9) Exogenous Epo enhances neo-vascularization(10) and improves ventricular function(11) in ischemic myocardium. Systemic Epo administration also attenuates hyperoxia-induced lung inflammation and injury. (12) These reports attest to the potent cytoprotective and pro-repair actions of the Epo-EpoR axis. However, a high Epo dose is required(13), which predisposes to serious systemic adverse effects. (2)

Compared to Epo, EpoR expression is even more rapidly and vigorously upregulated by metabolic stress, (14) associated with cytoprotection in several organs. (15, 16) Whereas low levels of Epo mRNA are normally present in the lung that do not change with anemia, and it is unclear whether Epo protein is actually locally produced in the lung, (17) we found abundant EpoR transcript and protein expression in the distal lung that is upregulated during development and further increased during post-pneumonectomy compensatory lung growth. (18–21) This suggest that the regulation of the Epo-EpoR axis in the lung may reside more at the receptor level. The effects of direct selective upregulation of pulmonary EpoR expression have not been examined. We hypothesized that local stimulation of pulmonary EpoR expression and signaling protects against lung injury. To test this hypothesis and ensure targeted sustained EpoR expression, we incorporated EpoR cDNA into biocompatible, biodegradable, polymeric nanoparticles (NPs) for delivery by nebulization into rat lung. Using magnetic tracer and tagged cDNA, we documented the *in vivo* pulmonary uptake and distribution of NPs, the time course of sustained EpoR expression and downstream signal transduction following nebulization. To fully explore the translational biomedical potential, separate animals received NPs containing EpoR cDNA by nebulization, and at peak pulmonary EpoR expression were exposed to hyperoxia. Control animals received vector-bearing NPs and/or were exposed to normoxia. The lungs were analyzed for morphology, edema and oxidative damage.

Methods

DNA constructs

Full-length human EpoR cDNA was cloned in the pMX-IRES-GFP expression vector (Cell Biolabs, San Diego, CA) upstream of the internal ribosome entry site (IRES) with a separate open reading frame co-expressing green fluorescent protein (EpoR-GFP) The level of GFP fluorescence from this vector is proportional over a 50-fold range to the level of expression of the protein encoded by the cDNA placed upstream of IRES. Full length canine EpoR cDNA (EpoR-FLAG) was cloned in the p3xFLAG-CMV-14 expression vector (Sigma-Aldrich, Milwaukee, WI) with 3 tandem FLAG epitopes (Asp-Tyr-Lys-Xaa-Xaa-Asp) in the C-terminus of EpoR.

Nanoparticles fabrication

We previously established poly-lactic-co-glycolic acid (PLGA) NPs as promising cDNA carriers for pulmonary delivery by inhalation. (22) PLGA is an FDA-approved, biocompatible and biodegradable polymer allowing controlled release of core compound. Using a solvent evaporation method, cDNA solution in DI water was added dropwise to a 3% w/v PLGA (Lakeshore Biomaterials, Birmingham, AL) solution prepared in chloroform to form a primary emulsion, which was then added to an aqueous solution of 5% w/v polyvinyl alcohol (PVA) to create double emulsion, sonicated, and stirred overnight at room temperature allowing the solvent to evaporate. The NPs were recovered by ultracentrifugation (25,000 rpm, 30 min, 10°C) and lyophilization.

Superparamagnetic iron oxide (SPIO) was used as a tracer for NP characterization. A 1% PLGA solution in dichloromethane (DCM) was prepared, then 10 mg of silanized (23) iron

oxide NPs (Meliorum technologies, Rochester, NY) was added and sonicated for 8 min at 20W. The oil or organic phase of the reaction was added dropwise to 5% PVA solution in de-ionized (DI) water to form the aqueous phase. The NP solution was sonicated for 10 min at 50 W, stirred overnight to remove the organic solvent, then centrifuged at 1000 rpm for 2 minutes to remove excess surfactant and iron oxide. The NPs were collected using a magnet, washed and lyophilized.

For cDNA loading, 10% w/w of cDNA was dispersed in DI water with glucose (1:1 ratio) as cryoprotectant for emulsification. Control NPs were loaded with empty vector. The prepared NPs were characterized (*below*) then lyophilized and stored until use.

Nanoparticle characterization

Following established procedures(22), particle size, poly-dispersity and surface charge were measured using dynamic light scattering (DLS) (ZetaPALS, Brookhaven Instruments, Holtsville, NY). The NP suspension was diluted, placed in a plastic cuvette and inserted into the DLS detector. Readings were obtained based on the Brownian motion of NPs within the solution. To visualize NP size and morphology, samples were prepared on a 200-mesh Formvar-coated copper grid and examined under transmission electron microscopy (TEM, FEI Tecnai G2 Spirit BioTWIN, Hillsboro, OR). Fourier transform infrared (FTIR) spectroscopy was performed using attenuated total reflectance technique without sample pretreatment (Nicolet 6700, Thermo Scientific, Waltham, MA); the instrument gives measurement from 500 cm^{-1} wave number. Iron content was assessed using a standard iron assay. (24) A superconducting quantum interference device (SQUID; Quantum Design) magnetometer was used to study the magnetic properties of SPIO-NPs embedded in epoxy resin beads at 25°C. (25) Particle stability was studied in DI water, 10% fetal bovine serum (FBS) and 0.9% saline over 5 days. The NP solutions were placed in a cuvette and incubated at 37°C. Particle size was measured every 24h using the DLS detector.

DNA loading efficiency and release

Loading efficiency (%) was calculated as: (Total DNA added – unencapsulated DNA in supernatant) × 100/total DNA added. To determine release profile, NPs containing cDNA were re-suspended in DI water (1mg/ml). Next, 1 ml of NP solution was added to a dialysis bag (100 kDa molecular weight cut-off, Spectrum Laboratories, Rancho Dominguez, CA) at 37°C for 28 days. At pre-determined time points, dialysates were collected (in −20°C) and replenished with fresh DI water; 4 replicated were used. The amount of cDNA released was quantified by UV absorbance (Infinite M200 plate reader, Tecan, San Jose, CA). A standard curve of known cDNA concentrations was used to determine cumulative DNA release.

Biocompatibility

Human alveolar type-1 epithelial cells (Applied Biological Materials, Richmond, BC) were seeded (5000 cells/well), incubated at 37°C for one day to establish cell adhesion, then incubated with increasing concentrations of NPs (up to 1000 μg/ml) at 37°C for 24 h. Following incubation, MTS assay (CellTiter 96®AQueous One Solution Cell Proliferation Assay, Promega, Madison, WI) was used to determine cell viability using a UV-Vis

spectrometer following manufacturer's instructions. Control cells were incubated without NPs.

Cellular uptake

Human type-1 alveolar epithelial cells were seeded (5000 cells/well) and incubated at 37°C for 1 h. To study dose-dependent cellular uptake, cells were incubated with increasing concentration of NPs (0 to 1000 μg/ml) for 1 h. To study time-dependent uptake, cells were incubated with SPIO- NPs at a fixed concentration (100 μg/ml) for varying duration (1, 2, 4 and 6 h). Following incubation, the cells were extensively washed to remove free NPs and lysed using 1X Triton. NP uptake was measured using iron assays normalized by the cell protein per well measured by Pierce BCA assay. All *in vitro* assays were performed in quadruplicates.

Animal studies

All animal protocols were conducted following the National Institutes of Health Guide for the Care and Use of Laboratory Animals, and approved by the Institutional Animal Care and Use Committee at UT Southwestern Medical Center.

To characterize tissue EpoR expression and signaling, Sprague-Dawley rats (~300g, Charles River Laboratories, Wilmington, MA) received nebulized NPs (2mg) encapsulating either human EpoR-GFP or empty vector (control) by inhalation (*below*). Time course of FLAG expression and EpoR signal transduction – total (t-) and phospho (p-) ERK1/2 and STAT5 in lung tissue were examined 4, 8, 14, and 21 days later.

To characterize the effect of EpoR expression on acute lung injury, separate rats received nebulized NPs (2mg) encapsulating either canine EpoR-FLAG or empty vector. Seven days later, animals were exposed to hyperoxia (90% inspired O_2) in an environmental chamber (Biospherix™, Lacona, NY) for 3 days. Control animals were exposed to normoxia (21% O_2) (4 animals each).

Inhalation delivery

Animals were anesthetized (ketamine 50mg/kg, xylazine 5mg/kg, i.p.) and intubated (14-gauge cannula). Heart rate and transcutaneous oxygen saturation were monitored via a tail cuff (Kent Scientific, Torrington, CT). The NPs were suspended in 0.5ml of sterile saline, sonicated for 2 min (300VT ultrasonic homogenizer, Biologics, Manassas, VA), immediately aerosolized using a vibrating mesh nebulizer (4–6μm droplets, Aeroneb™, Aerogen, Galway, Ireland), and delivered via the tracheal cannula over 3 min. The animal was observed following nebulization until recovery from anesthesia.

Magnetic resonance imaging (MRI)

To detect *in vivo* distribution of inhaled aerosolized SPIO-NPs, MRI was conducted in a 3T whole-body human scanner (Achieva™, Philips Medical Systems, Best, Netherlands) with a small solenoid coil (I.D. 63mm) (26). The animal was anesthetized with 1.5 to 2% isoflurane and placed in the supine position while breathing medical grade air spontaneously through a respiratory mask. The entire lung was imaged with a three-dimensional ultra-short echo time

(UTE) sequence: TE 90μs, pulse repetition time 10ms, radiofrequency pulse flip angle 10°, field of view 70^3 mm^3, image matrix size 100^3 (reconstructed to 260μm isotropic resolution), number of excitation 1.

Lung harvest

Rats were killed by intraperitoneal overdose injection of pentobarbital (86mg/kg) and phenytoin (11mg/kg). The left lung was removed and flushed clear of blood. Samples were taken and snap frozen in liquid nitrogen. The right lung was fixed by tracheal instillation of 4% paraformaldehyde at 25 cmH_2O of airway pressure. The fixed lung was removed and immersed in 4% paraformaldehyde for at least 2 weeks. Each lobe was serially sliced (3mm) and the slice faces imaged using a biofluorescence imager (CRI Maestro 2, Cambridge Research & Instrumentation, Waltham, MA; excitation/emission wavelengths, 475/509nm). Tissue blocks embedded in paraffin were sectioned (4μm) and examined under a fluorescence microscope (Zeiss LSM510). Trichrome stained sections were examined under light microscopy.

Fluorescent microscopy and immunohistochemistry

Cryosections (4μm) were prepared from frozen lung samples, rinsed (0.1% TritonX-100 in PBS), blocked (1.5% BSA, 10% goat serum in PBS), and incubated with primary antibody (1:200): Rat anti-FLAG M2 (Agilent Technologies, Santa Clara, CA; Cat#200471), rabbit monoclonal anti-p-ERK1/2, anti-t-ERK1/2 and anti-p-STAT5 (Cell Signaling Technology, Beverly, MA; Cat#4695, 4695 and 9359, respectively), and rabbit polyclonal IgG anti-t-STAT5 (Santa Cruz, San Diego, CA, Cat#:sc-835). The sections were rinsed and incubated with Alexa Fluor-546 conjugated secondary antibody (1:1000, Invitrogen, Eugene, OR). Fluorescent phalloidin-488 (Invitrogen) was used for actin staining and SYTO-61 (Invitrogen) for nuclei staining. The sections were viewed under confocal microscopy (Carl Zeiss LSM 510).

Immunoblot

Lung tissue (~50mg) was homogenized in 300μL of RIPA buffer [150 mM NaCl, 50 mM Tris·HCl, pH 7.4, 5 mM EDTA, 1% Triton X-100, 0.5% deoxycholate, and 0.1% SDS] containing fresh phosphatase inhibitors and protease inhibitors and cleared by centrifugation (14,000g, 4°C, 30 min), and protein content determined by the Bradford method. Protein samples (~30μg per lane) were fractionated by SDS-PAGE, transferred to PVDF membrane, blocked by nonfat milk, and probed with primary antibodies (see previous paragraph), followed by horseradish peroxidase-conjugated goat anti-rabbit secondary antibody. Labeling was detected by autoradiography and enhanced chemiluminescence. β-actin served as loading control.

Injury assessment

Apoptosis: Caspase-8 activity was measured by colorimetric assay (ApoAlert™, Clontech, Mountain View, CA). *Total antioxidant capacity*: Copper-reducing equivalents (CRE) were measured by calorimetric assay (OxiSelect™, Cell BioLabs, San Diego, CA). *DNA damage*: DNA was extracted using DNAzol™ (Life Technologies, Grand Island, NY), precipitated in

100% ethanol, washed with 70% ethanol and suspended in 8mM NaOH, The 8-hydroxy-2′-deoxyguanosine (8-OHdG) level was measured by ELISA (OxiSelect™, Cell BioLabs). *Protein oxidation*: Protein Carbonyl level was measured by ELISA (OxiSelect™ Cell BioLabs). *Lipid oxidation*: 8-isoprostane level was measured by EIA (Cayman Chemical, Ann Arbor, MI). *Edema estimation*: Lung tissue (~100mg) was weighed and transferred to a platinum ashing crucible on a hot plate (100°C) under a heat lamp for 2h. The sample-containing crucible was weighed to determine the sample dry weight. The crucible was placed overnight in the oven (600°C) and the ash weight determined. The ash was dissolved in 2mL of HCl and the sodium content measured by flame photometry. Sodium-to-dry weight ratio is a surrogate marker for the relative amount of interstitial fluid (extracellular/intracellular sodium concentration: 135–140/10–15 mM). Assays were performed in triplicates.

Data analysis

Results (mean±SD) were compared across conditions by two-way ANOVA with post-hoc Fisher's protected least significant difference test. Temporal changes in expression were evaluated by p trend. EpoR expression was normalized to that on Day 4 (set as 100%). Expression of p/t-ERK1/2 and p/t-STAT5 was normalized to that of control (vector only) NPs (set as 100%). Using a Random Effects Model (27) to account for the correlated observations within each experiment from day 4 to day 21, point and interval estimates (95% CI) for p/t-ERK1/2 and p/t-STAT5 levels were determined to assess whether the expression increased beyond control level. $P<0.05$ was considered significant.

Results

Nanoparticle characterization

Hydrodynamic diameter of PLGA NPs was <200nm and SPIO-NPs was 250nm (Table 1); the superparamagnetic behavior of our SPIO-NPs concurs with that in previous reports. (28, 29) Loading efficiency was 41±5% (mean±SD). Under TEM, NPs without SPIO are smooth and spherical (Figure 1A) while SPIO-containing NPs (11.8% iron content by weight) are spiculated with the iron oxide particles present in the core as well as evenly distributed on the surface (Figure 1B). TEM confirmed the particle size obtained using DLS. FTIR spectra of SPIO-NPs (Figure 1C) showed characteristic stretching of –OH within carboxylic acid groups (3320 cm^{-1}) and C=O bonds (1710 cm^{-1}) which represent carbonyl groups of the ester linkages within PLGA compared to the spectra of naked iron oxide NPs (Fe-O peak at 590 cm^{-1}) (30, 31) and PLGA (C=O stretching at 1735 cm^{-1}, C-O stretching at 1072 cm^{-1}) SQUID magnetometry (Figure 1D) showed a decrease in saturation magnetization of SPIO-NPs compared to naked SPIO. At low magnetic field SPIO-NP superparamagnetic properties (remanence 0.022, coercivity 69.8) are similar to that of bare SPIO (0.028 and 75.4, respectively).

Payload release, cytocompatibility, and uptake by lung epithelial cells

In de-ionized water, NPs showed a 32±8% burst release of the encapsulated agents within 2 days, followed by sustained release of 76±4% over 28 days (Figure 2A). Alveolar epithelial cells incubated with SPIO-NPs for 24 h show >90% viability up to a NP concentration of

500 μg/ml, with >80% viability at 1000 μg/ml (Figure 2B). NP uptake by human alveolar epithelial cells within 1 h of incubation was concentration-dependent up to 300μg/ml NP (Figure 2C). At a NP concentration of 100 μg/ml, uptake by alveolar epithelial cells saturated at 2 h of incubation, indicating time-dependence (Figure 2D).

In vivo uptake, distribution and signal transduction

Two hours following inhalation of nebulized SPIO-NPs, widespread pulmonary distribution was shown by the diffusely lower MR signal intensity of lung parenchyma compared to that in simultaneous saline-treated or untreated control lungs, consistent with the known "negative contrast" effect of SPIO (Figure 3A). (32) Under light microscopy, scattered Prussian blue staining of iron oxide was seen in alveolar septal cells and macrophages (Figure 3B). Under TEM, SPIO-NPs in various stages of degradation and disseminated free iron oxide particles were visualized within alveolar septal cells (Figure 3C).

Inhalation of aerosolized NPs encapsulating EpoR-GFP DNA resulted in progressively increased tissue fluorescence over 21 days in all rat lobes (Figure 4A). Inhalation of aerosolized NPs encapsulating EpoR-FLAG DNA resulted in increasing EpoR-FLAG expression that peaked around day 10 and remained elevated above baseline up to day 21 (Figure 4B–D). Figure 4D shows the time course of several experiments normalized to the expression level on Day 4, which was a common time point for all series of experiments. The variable expression levels were partly due to inter-animal variation but mostly explained by regional sampling variations due to the fact that each lane represents signal from a very small piece of lung tissue.

Corresponding to the EpoR expression is functional evidence of EpoR activity *in vivo*. We found increased phosphorylation of ERK1/2 and STAT5 (Figure 5A–C), consistent with upregulation of EpoR signal transduction. Note that both of these downstream signals were elevated in a sustained fashion, peaking around day 10 and remaining elevated above control up to day 21 with mean levels of 219% (95% CI: 150%–289%) and 190% (95% CI: 123%–257%) respectively; which are congruent with the time course of exogenous EpoR expression.

EpoR cDNA delivery in hyperoxic lung injury

In animals receiving NPs containing EpoR-FLAG cDNA compared to those receiving NPs containing vector only, the expected hyperoxia-induced alveolar septal thickening, tissue edema and cell/fluid exudation were significantly reduced as assessed by morphology (Figure 6A), and the wet/dry weight and Na^+/dry weight ratios (Figure 6B). Inhalation of EpoR cDNA attenuated hyperoxia-induced apoptosis measured from caspase-8 activity (Figure 6C) and ameliorated the increases in tissue oxidative DNA damage measured from 8-OHdG level (Figure 6C), protein oxidation measured from protein carbonyl level (Figure 6D) and, lipid oxidation measured from 8-isoprostane level (Figure 6D). In contrast, EpoR cDNA treatment had no effect on the hyperoxia-induced increase in total anti-oxidant capacity measured from copper reducing equivalents (per mg protein, mean±SD: Normoxia + plasmid control 9.5±2.0; Hyperoxia + plasmid control 19.8±2.3; Normoxia + EpoR

9.2±2.1; Hyperoxia + EpoR 20.9±2.0. P<0.01 by ANOVA, normoxia vs. hyperoxia. NS plasmid control vs. EpoR).

Discussion

Summary of the main findings

This is the first report using nanoparticle-facilitated, targeted inhalational gene delivery to directly upregulate an endogenous pleiotropic receptor in the lung and effectively enhances cytoprotection from an external insult. We demonstrated that 1) PLGA NPs encapsulating DNA and/or magnetic or fluorescent labels are stable (results not shown), biocompatible, and rapidly taken up by lung epithelial cells, with a sustained payload release profile. 2) Inhalation of aerosolized NPs results in widespread distribution of the encapsulated agent within lung cells, detected using various imaging techniques, with sustained gene expression for up to 21 days after a single treatment. 3) Inhalation of NPs containing EpoR cDNA successfully increases EpoR protein expression in the distal lung. 4) Increasing EpoR expression activates canonical EpoR signaling pathways, attenuates hyperoxia-induced apoptosis, oxidative stress damage of DNA, protein and lipid, ameliorates alveolar septal edema, and preserves alveolar morphology. These results establish a viable delivery system, the therapeutic effectiveness of NP-facilitated DNA delivery to the lung, and the efficacy of targeted manipulation of EpoR signaling in ameliorating acute oxidant lung damage.

Pulmonary delivery of DNA-laden nanoparticles

We previously screened several natural and synthetic polymers as carriers for protein and DNA delivery to the lung, and found that PLGA exhibits the most favorable physical and biological characteristics. (22) PLGA is widely used owing to its biocompatibility, biodegradability and sustained drug release profile. (33) PLGA-based NPs loaded with deoxyribonuclease I have been nebulized to treat various lung diseases. (34, 35) PLGA microspheres (~2μm) containing rifampicin have been nebulized for the treatment of tuberculosis. (36) Pulmonary delivery of insulin-loaded PLGA NPs (400nm) in guinea pigs significantly prolongs hypoglycemic effect compared to nebulized aqueous free insulin solution. (37) Our PLGA NPs incorporating DNA with or without tracers demonstrate physical properties that concur with PLGA-magnetite NPs fabricated by others, (25) and are stable without aggregation in various solutions. The bi-phasic release of core compound – an initial burst release of 32±8% within 2 days followed by a sustained release of 76±4% over 3 weeks – is characteristic of PLGA-based NPs. (38) Release occurs via bulk erosion of PLGA by the hydrolysis of ester bonds. The release profile of PLGA NPs may be customized by varying parameters such as the ratio of poly-lactic acid to poly-glycolic acid, porosity, and crystallinity. (39) We found excellent lung epithelial cell viability with PLGA NPs bearing SPIO or DNA. The dose- and time-dependent uptake of our NPs by alveolar epithellial cells concurs with previous reports of PLGA NP uptake by airway, gut and renal epithelial cells (40) as well as human umbilical vein endothelial cells, (41) and the uptake of poly(dl-lactic acid-co-α, β-malic acid)-magnetite composite NPs by human mesenchymal stem cells. (42)

Nanoparticle as gene carrier to the lung

While PLGA NPs have been used for tracheal delivery of small molecules such as pirfenidone for anti-fibrotic effects against bleomycin pulmonary fibrosis in mice, (43) to our knowledge this is the first study to document the time course of PLGA NP-facilitated DNA delivery by nebulization and characterization of the *in vivo* pulmonary expression and action. We previously showed that inhalation of PLGA NPs bearing enhanced yellow fluorescent protein (eYFP) cDNA increased pulmonary eYFP expression for 7 days; longer time points were not examined. (22) Because commercial EpoR antibodies are of questionable specificity, we tagged EpoR with FLAG or co-expressed GFP as markers for EpoR expression as well as measured two major downstream signal transduction pathways (ERK1/2 and STAT5). Using GFP as a marker, fluorescent protein expression following NP nebulization increased steadily for at least 21 days. Using FLAG tag, the increase in EpoR-FLAG protein expression peaked by days 10 then began to decline, although expression remained elevated significantly above baseline up to day 21 and corresponded to the time course of upregulation in EpoR signal transduction. The difference in expression pattern of GFP and FLAG is likely related to the inherent long half-life of GFP. The inter-experiment variability in EpoR expression and signaling is likely due to regional variations within the lung and random tissue sampling for immunoblots.

Nanoparticles as tracer

In addition to the labeled DNA, we used SPIO as a magnetic tracer to image the pulmonary distribution of inhaled NPs *in vivo* and *ex vivo*, and from macro- to micro-scales. SPIO-loaded NPs are stable and biocompatible. They maintained acceptable superparamagnetic properties in spite of a lower saturation magnetization (34.79 emu/g) compared to bare SPIO (67.48 emu/g) at room temperature. This decrease could be attributed to the noncollinear spin distribution usually observed at particle surface (28) and/or the presence of nonmagnetic polymer coating. However, the values observed by us are within the range acceptable for drug delivery applications. (44) Magnetic NPs with saturation magnetization as low as 7–8 emu/g show attraction towards small magnets, which supports their experimental use as targeting contrast agents. (45) SPIO has been used as a “negative” MRI contrast agent owing to its effect of shortening the effective transverse relaxation time (T2*) causing a reduction of signal intensity. (32) We demonstrated this effect by UTE MRI, which confirmed widespread SPIO distribution throughout lung parenchyma. SPIO is also widely visualized *ex vivo* within alveolar septa by light microscopy, and within lung cells by TEM. Thus, SPIO-NPs are a versatile tool for preclinical development and imaging of inhalation drugs.

Lung protection by EpoR

EpoR is a single transmembrane protein of the cytokine class I receptor family and signals through various protein kinases and transcription factors. EpoR is ubiquitously expressed (46) and exists as a homodimer with Epo binding asymmetrically to the extracellular domain. Epo binding induces EpoR dimerization, triggering auto-phosphorylation and activating the Janus family protein tyrosine kinase JAK-2, leading to phosphorylation of tyrosine residues in the intracellular C-terminal tail of EpoR followed by activation of

signaling molecules including the signaling molecules ERK1/2 and transcription factor STAT5, among others. (47) Paracrine/autocinre EpoR signaling is multi-functional, promoting anti-apoptosis, progenitor cell recruitment and differentiation, angiogenesis, and organ development while protecting against ischemic/hypoxic injury in a tissue-specific manner. (48–51) In addition, a high EpoR expression in tumors is a favorable prognostic factor. (52)

In the lung, EpoR transcript is widely expressed. Expression is upregulated in actively growing lungs of developing animals, and further increased post-pneumonectomy during accelerated compensatory lung growth in response to mechanical stress imposed on the remaining lung, acting in part through the hypoxia-inducible factor-1α (HIF-1α), a transcriptional regulator of Epo-EpoR signaling. (18–21) Our results showing significant EpoR protection against oxidant stress damage in the lung is consistent with that reported in the kidney. In renal cells, knockdown of endogenous EpoR increases susceptibility while EpoR overexpression increases resistance to peroxide-induced oxidative damage. *In vivo* EpoR expression protects kidneys against ischemia reperfusion injury, signaling at least partly downstream of Klotho. (16) In the lung, the effects of upregulated EpoR expression by cDNA inhalation – minimizing alveolar cellular apoptosis, DNA, protein and lipid oxidation as well as tissue edema – are similar to that following systemic supplementation with Klotho-containing conditioned medium;(53) however, unlike Klotho, enhancing EpoR expression does not increase total endogenous anti-oxidant capacity (unpublished observations), suggesting different mechanisms of action between the two pleiotropic cytoprotective pathways.

In conclusion, we established the feasibility and efficacy of nanoparticle-facilitated inhalational delivery of nebulized EpoR cDNA to the lung, documented the release and distribution of exogenous EpoR cDNA, the sustained expression and signaling of EpoR in lung parenchyma, and the efficacy in pulmonary cytoprotection and amelioration of oxidative damage. The advantage of PLGA NPs in inhalational DNA delivery includes its ease of synthesis, stability of the preparation, rapid cell uptake, high biocompatibility, and prolonged payload release and action, which should reduce dose and frequency requirements, minimize systemic adverse effects and improve the cost-benefit ratio of treatment, making it a practical and effective non-invasive formulation for translational development. Future studies will examine cytoprotection by EpoR and many candidates (small molecules, recombinant protein, biosimilars, cDNA) in more chronic models of oxidative lung injury, optimize the dose and frequency of administration, and monitor long-term effects of repetitive dosing.

Acknowledgments

This work was supported by the National Heart, Lung and Blood Institute Grants R01 HL40070 (CCH) U01 HL111146 (CCH, KTN) and HL110967 (CCH), and the National Institute of Diabetes, Digestive and Kidney Diseases grants R01-DK091392 and DK092461 (both OWM), the Charles and Jane Pak Foundation (OWM), and the O'Brien Kidney Research Center (P30-DK-07938) (OWM).

We acknowledge the assistance of UT Southwestern Imaging Core Facility and Dr. Jiechao Jiang at the Materials Science Department of the University of Texas at Arlington for the use of their instruments for TEM characterization. We also appreciate the technical assistance of the staff of the Animal Resources Center at UT

Southwestern Medical Center, and Beverly Huet-Adams of the Department of Clinical Science for statistical advice.

References

1. Johnson ER, Matthay MA. Acute lung injury: epidemiology, pathogenesis, and treatment. J Aerosol Med Pulm Drug Deliv. 2010; 23:243–252. [PubMed: 20073554]
2. Brines M, Cerami A. Erythropoietin-mediated tissue protection: reducing collateral damage from the primary injury response. J Intern Med. 2008; 264:405–432. [PubMed: 19017170]
3. Jaquet K, Krause K, Tawakol-Khodai M, Geidel S, Kuck K. Erythropoietin and VEGF exhibit equal angiogenic potential. Microvasc Res. 2002; 64:326. [PubMed: 12204656]
4. Wang L, Zhang Z, Wang Y, Zhang R, Chopp M. Treatment of stroke with erythropoietin enhances neurogenesis and angiogenesis and improves neurological function in rats. Stroke; a journal of cerebral circulation. 2004; 35:1732–1737.
5. Jelkmann W, Bohlius J, Hallek M, Sytkowski AJ. The erythropoietin receptor in normal and cancer tissues. Crit Rev Oncol Hematol. 2008; 67:39–61. [PubMed: 18434185]
6. Burger D, Xenocostas A, Feng QP. Molecular basis of cardioprotection by erythropoietin. Curr Mol Pharmacol. 2009; 2:56–69. [PubMed: 20021446]
7. Xu K, George I, Klotz S, Hay I, Xydas S, Zhang G, Cerami A, Wang J. Erythropoietin derivate improves left ventricular systolic performance and attenuates left ventricular remodeling in rats with myocardial infarct-induced heart failure. J Cardiovasc Pharmacol. 2010; 56:506–512. [PubMed: 20881614]
8. Chua S, Leu S, Lin YC, Sheu JJ, Sun CK, Chung SY, Chai HT, Lee FY, Kao YH, Wu CJ, et al. Early erythropoietin therapy attenuates remodeling and preserves function of left ventricle in porcine myocardial infarction. J Investig Med. 2011; 59:574–586.
9. Calvillo L, Latini R, Kajstura J, Leri A, Anversa P, Ghezzi P, Salio M, Cerami A, Brines M. Recombinant human erythropoietin protects the myocardium from ischemia-reperfusion injury and promotes beneficial remodeling. Proc Natl Acad Sci U S A. 2003; 100:4802–4806. [PubMed: 12663857]
10. Wang T, Jiang XJ, Lin T, Ren S, Li XY, Zhang XZ, Tang QZ. The inhibition of postinfarct ventricle remodeling without polycythaemia following local sustained intramyocardial delivery of erythropoietin within a supramolecular hydrogel. Biomaterials. 2009; 30:4161–4167. [PubMed: 19539990]
11. Taniguchi N, Nakamura T, Sawada T, Matsubara K, Furukawa K, Hadase M, Nakahara Y, Matsubara H. Erythropoietin prevention trial of coronary restenosis and cardiac remodeling after ST-elevated acute myocardial infarction (EPOC-AMI): a pilot, randomized, placebo-controlled study. Circ J. 2010; 74:2365–2371. [PubMed: 20834185]
12. Lee JH, Sung DK, Koo SH, Shin BK, Hong YS, Son CS, Lee JW, Chang YS, Park WS. Erythropoietin attenuates hyperoxia-induced lung injury by down-modulating inflammation in neonatal rats. J Korean Med Sci. 2007; 22:1042–1047. [PubMed: 18162720]
13. Prunier F, Pfister O, Hadri L, Liang L, Del Monte F, Liao R, Hajjar RJ. Delayed erythropoietin therapy reduces post-MI cardiac remodeling only at a dose that mobilizes endothelial progenitor cells. Am J Physiol Heart Circ Physiol. 2007; 292:H522–529. [PubMed: 16997893]
14. Spandou E, Papoutsopoulou S, Soubasi V, Karkavelas G, Simeonidou C, Kremenopoulos G, Guiba-Tziampiri O. Hypoxia-ischemia affects erythropoietin and erythropoietin receptor expression pattern in the neonatal rat brain. Brain Res. 2004; 1021:167–172. [PubMed: 15342264]
15. Chen ZY, Wang L, Asavaritkrai P, Noguchi CT. Up-regulation of erythropoietin receptor by nitric oxide mediates hypoxia preconditioning. J Neurosci Res. 2010; 88:3180–3188. [PubMed: 20806411]
16. Hu MC, Shi M, Cho HJ, Zhang J, Pavlenco A, Liu S, Sidhu S, Huang LJ, Moe OW. The erythropoietin receptor is a downstream effector of Klotho-induced cytoprotection. Kidney International. 2013; 84:468–481. [PubMed: 23636173]
17. Fandrey J, Bunn HF. In vivo and in vitro regulation of erythropoietin mRNA: measurement by competitive polymerase chain reaction. Blood. 1993; 81:617–623. [PubMed: 8381307]

18. Foster DJ, Moe OW, Hsia CC. Upregulation of erythropoietin receptor during postnatal and postpneumonectomy lung growth. Am J Physiol Lung Cell Mol Physiol. 2004; 287:L1107–1115. [PubMed: 15286000]
19. Zhang Q, Bellotto DJ, Ravikumar P, Moe OW, Hogg RT, Hogg DC, Estrera AS, Johnson RL Jr, Hsia CC. Postpneumonectomy lung expansion elicits hypoxia-inducible factor-1alpha signaling. Am J Physiol Lung Cell Mol Physiol. 2007; 293:L497–504. [PubMed: 17513452]
20. Zhang Q, Moe OW, Garcia JA, Hsia CC. Regulated expression of hypoxia-inducible factors during postnatal and postpneumonectomy lung growth. Am J Physiol Lung Cell Mol Physiol. 2006; 290:L880–889. [PubMed: 16373673]
21. Zhang Q, Zhang J, Moe OW, Hsia CC. Synergistic upregulation of erythropoietin receptor (EPO-R) expression by sense and antisense EPO-R transcripts in the canine lung. Proc Natl Acad Sci USA. 2008; 105:7612–7617. [PubMed: 18495932]
22. Menon JU, Ravikumar P, Pise A, Gyawali D, Hsia CC, Nguyen KT. Polymeric nanoparticles for pulmonary protein and DNA delivery. Acta biomaterialia. 2014; 10:2643–2652. [PubMed: 24512977]
23. Rahimi M, Yousef M, Cheng Y, Meletis EI, Eberhart RC, Nguyen K. Formulation and characterization of a covalently coated magnetic nanogel. Journal of nanoscience and nanotechnology. 2009; 9:4128–4134. [PubMed: 19916419]
24. Rahimi M, Wadajkar A, Subramanian K, Yousef M, Cui W, Hsieh J-T, Nguyen KT. In vitro evaluation of novel polymer-coated magnetic nanoparticles for controlled drug delivery. Nanomedicine. 2010; 6:672–680. [PubMed: 20172050]
25. Wadajkar AS, Bhavsar Z, Ko C-Y, Koppolu B, Cui W, Tang L, Nguyen KT. Multifunctional particles for melanoma-targeted drug delivery. Acta Biomater. 2012; 8:2996–3004. [PubMed: 22561668]
26. Takahashi M, Togao O, Obara M, van Cauteren M, Ohno Y, Doi S, Kuro-o M, Malloy C, Hsia CC, Dimitrov I. Ultra-short echo time (UTE) MR imaging of the lung: comparison between normal and emphysematous lungs in mutant mice. J Magn Reson Imaging. 2010; 32:326–333. [PubMed: 20677258]
27. Laird NM, Ware JH. Random-effects models for longitudinal data. Biometrics. 1982; 38:963–974. [PubMed: 7168798]
28. Ding Y, Hu Y, Zhang L, Chen Y, Jiang X. Synthesis and Magnetic Properties of Biocompatible Hybrid Hollow Spheres. Biomacromolecules. 2006; 7:1766–1772. [PubMed: 16768396]
29. Lee P-W, Hsu S-H, Wang J-J, Tsai J-S, Lin K-J, Wey S-P, Chen F-R, Lai C-H, Yen T-C, Sung H-W. The characteristics, biodistribution, magnetic resonance imaging and biodegradability of superparamagnetic core-shell nanoparticles. Biomaterials. 2010; 31:1316–1324. [PubMed: 19959224]
30. Zhu X-M, Wang Y-XJ, Leung KC-F, Lee S-F, Zhao F, Wang D-W, Lai JMY, Wan C, Cheng CHK, Ahuja AT. Enhanced cellular uptake of aminosilane-coated superparamagnetic iron oxide nanoparticles in mammalian cell lines. International Journal of Nanomedicine. 2012; 7:953–964. [PubMed: 22393292]
31. Elizabeth AO, Tonya MA, Dustin AG, Susan MK, Kai L, Angelique YL. Rapid microwave-assisted synthesis of dextran-coated iron oxide nanoparticles for magnetic resonance imaging. Nanotechnology. 2012; 23:215602. [PubMed: 22551699]
32. McCullough BJ, Kolokythas O, Maki JH, Green DE. Ferumoxytol in clinical practice: implications for MRI. Journal of Magnetic Resonance Imaging. 2013; 37:1476–1479. [PubMed: 23097302]
33. Makadia HK, Siegel SJ. Poly Lactic-co-Glycolic Acid (PLGA) as biodegradable controlled drug delivery carrier. Polymers. 2011; 3:1377–1397. [PubMed: 22577513]
34. Osman R, Kan PL, Awad G, Mortada N, El-Shamy A-E, Alpar O. Enhanced properties of discrete pulmonary deoxyribonuclease I (DNaseI) loaded PLGA nanoparticles during encapsulation and activity determination. Int J Pharm. 2011; 408:257–265. [PubMed: 21335080]
35. Azarmi S, Roa WH, Lobenberg R. Targeted delivery of nanoparticles for the treatment of lung diseases. Adv Drug Deliv Rev. 2008; 60:863–875. [PubMed: 18308418]

36. Hirota K, Hasegawa T, Nakajima T, Inagawa H, Kohchi C, Soma G-I, Makino K, Terada H. Delivery of rifampicin-PLGA microspheres into alveolar macrophages is promising for treatment of tuberculosis. J Control Release. 2010; 142:339–346. [PubMed: 19951729]
37. Kawashima Y, Yamamoto H, Takeuchi H, Fujioka S, Hino T. Pulmonary delivery of insulin with nebulized dl-lactide/glycolide copolymer (PLGA) nanospheres to prolong hypoglycemic effect. J Control Release. 1999; 62:279–287. [PubMed: 10518661]
38. Menon JU, Kona S, Wadajkar AS, Desai F, Vadla A, Nguyen KT. Effects of surfactants on the properties of PLGA nanoparticles. J Biomed Mater Res A. 2012; 100:1998–2005. [PubMed: 22566409]
39. Alexis F. Factors affecting the degradation and drug-release mechanism of poly(lactic acid) and poly[(lactic acid)-co-(glycolic acid)]. Polym Int. 2005; 54:36–46.
40. Cartiera MS, Johnson KM, Rajendran V, Caplan MJ, Saltzman WM. The uptake and intracellular fate of PLGA nanoparticles in epithelial cells. Biomaterials. 2009; 30:2790–2798. [PubMed: 19232712]
41. Davda J, Labhasetwar V. Characterization of nanoparticle uptake by endothelial cells. Int J Pharm. 2002; 233:51–59. [PubMed: 11897410]
42. Wang L, Neoh K-G, Kang E-T, Shuter B, Wang S-C. Biodegradable magnetic-fluorescent magnetite/poly(dl-lactic acid-co-alpha, beta-malic acid) composite nanoparticles for stem cell labeling. Biomaterials. 2010; 31:3502–3511. [PubMed: 20144844]
43. Trivedi R, Redente EF, Thakur A, Riches DW, Kompella UB. Local delivery of biodegradable pirfenidone nanoparticles ameliorates bleomycin-induced pulmonary fibrosis in mice. Nanotechnology. 2012; 23:505101. [PubMed: 23186914]
44. Cheng F-Y, Su C-H, Yang Y-S, Yeh C-S, Tsai C-Y, Wu C-L, Wu M-T, Shieh D-B. Characterization of aqueous dispersions of Fe3O4 nanoparticles and their biomedical applications. Biomaterials. 2005; 26:729–738. [PubMed: 15350777]
45. Xu C, Xu K, Gu H, Zhong X, Guo Z, Zheng R, Zhang X, Xu B. Nitrilotriacetic acid-modified magnetic nanoparticles as a general agent to bind histidine-tagged proteins. J Am Chem Soc. 2004; 126:3392–3393. [PubMed: 15025444]
46. Constantinescu SN, Ghaffari S, Lodish HF. The Erythropoietin Receptor: Structure, Activation and Intracellular Signal Transduction. Trends Endocrinol Metab. 1999; 10:18–23. [PubMed: 10322390]
47. Richmond TD, Chohan M, Barber DL. Turning cells red: signal transduction mediated by erythropoietin. Trends Cell Biol. 2005; 15:146–155. [PubMed: 15752978]
48. Kertesz N, Wu J, Chen TH, Sucov HM, Wu H. The role of erythropoietin in regulating angiogenesis. Dev Biol. 2004; 276:101–110. [PubMed: 15531367]
49. Yu X, Lin CS, Costantini F, Noguchi CT. The human erythropoietin receptor gene rescues erythropoiesis and developmental defects in the erythropoietin receptor null mouse. Blood. 2001; 98:475–477. [PubMed: 11435319]
50. Balasubramaniam V, Mervis CF, Maxey AM, Markham NE, Abman SH. Hyperoxia reduces bone marrow, circulating, and lung endothelial progenitor cells in the developing lung: implications for the pathogenesis of bronchopulmonary dysplasia. Am J Physiol Lung Cell Mol Physiol. 2007; 292:L1073–1084. [PubMed: 17209139]
51. Satoh K, Kagaya Y, Nakano M, Ito Y, Ohta J, Tada H, Karibe A, Minegishi N, Suzuki N, Yamamoto M, et al. Important role of endogenous erythropoietin system in recruitment of endothelial progenitor cells in hypoxia-induced pulmonary hypertension in mice. Circulation. 2006; 113:1442–1450. [PubMed: 16534010]
52. Rozsas A, Berta J, Rojko L, Horvath LZ, Keszthelyi M, Kenessey I, Laszlo V, Berger W, Grusch M, Hoda MA, et al. Erythropoietin receptor expression is a potential prognostic factor in human lung adenocarcinoma. PLoS One. 2013; 8:e77459. [PubMed: 24155958]
53. Ravikumar P, Ye J, Zhang J, Pinch SN, Hu MC, Kuro OM, Hsia CC, Moe OW. alpha-Klotho protects against oxidative damage in pulmonary epithelia. Am J Physiol Lung Cell Mol Physiol. 2014; 307:L566–575. [PubMed: 25063799]

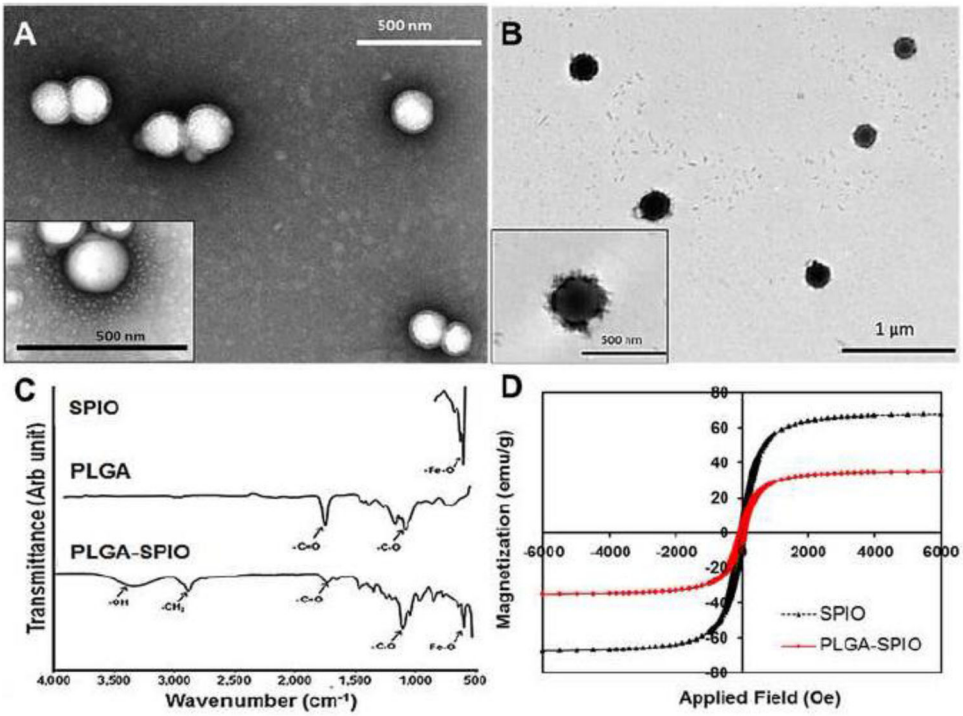

Figure 1.

Nanoparticle (NP) characterization. TEM images show **(A)** PLGA and **(B)** PLGA-SPIO-NPs. **C)** FTIR spectra of bare iron oxide NPs (Fe-O peak at 590 cm^{-1}), PLGA (C=O stretching at 1735 $cm^{-1}$and C-O stretching at 1072 cm^{-1}) and PLGA-SPIO-NPs (OH stretching at 3320 cm^{-1}, C=O peak at 1710 $cm^{-1}$and Fe-O peak at 580 cm^{-1}). **(D)** Hysteresis loops of bare SPIO and PLGA-SPIO-NPs indicate a decrease in magnetization of polymer-bound iron oxide NPs. The coercivity and remanence values are within the range suitable for magnetic-based drug delivery.

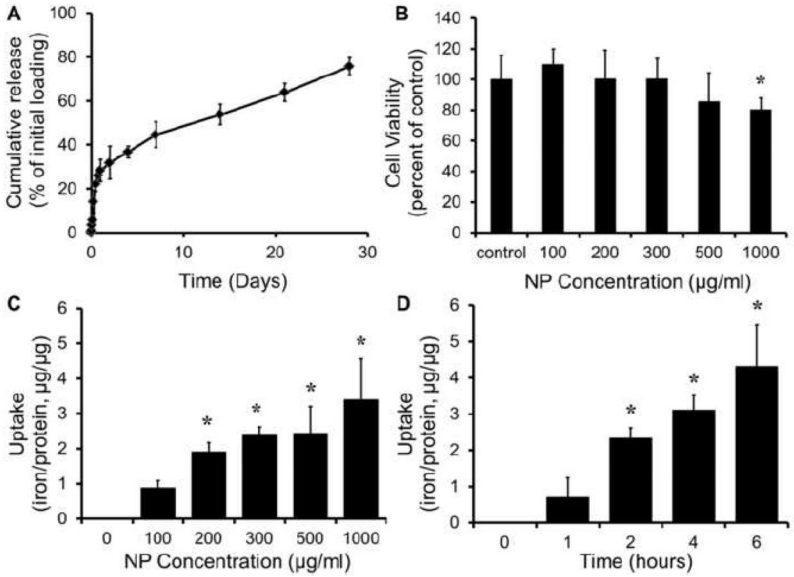

Figure 2.

(A) Release of human EpoR-GFP cDNA from PLGA NPs (1mg/ml) incubated at 37°C was analyzed by absorbance measurements. An initial burst release of 32±8% of encapsulated cDNA was observed within 2 days followed by sustained release up to 28 days. **(B)** Cytocompatibility of SPIO-NPs incubated with human alveolar type-1 epithelial cells for 24 h was analyzed using MTS assays (n=4). Greater than 80% cell viability was observed up to 500μg/ml of NP concentration. **(C)** Dose-dependent uptake of SPIO-NPs by human alveolar type-1 epithelial cells was analyzed using iron and BCA protein assays after 1 h of incubation. **(D)** Time-dependent uptake of SPIO-NPs (100μg/ml) by human alveolar type-1 epithelial cells over 6 h was analyzed using iron and BCA assays. Mean±SD of 4 replicates. *$p<0.05$ vs. control (zero).

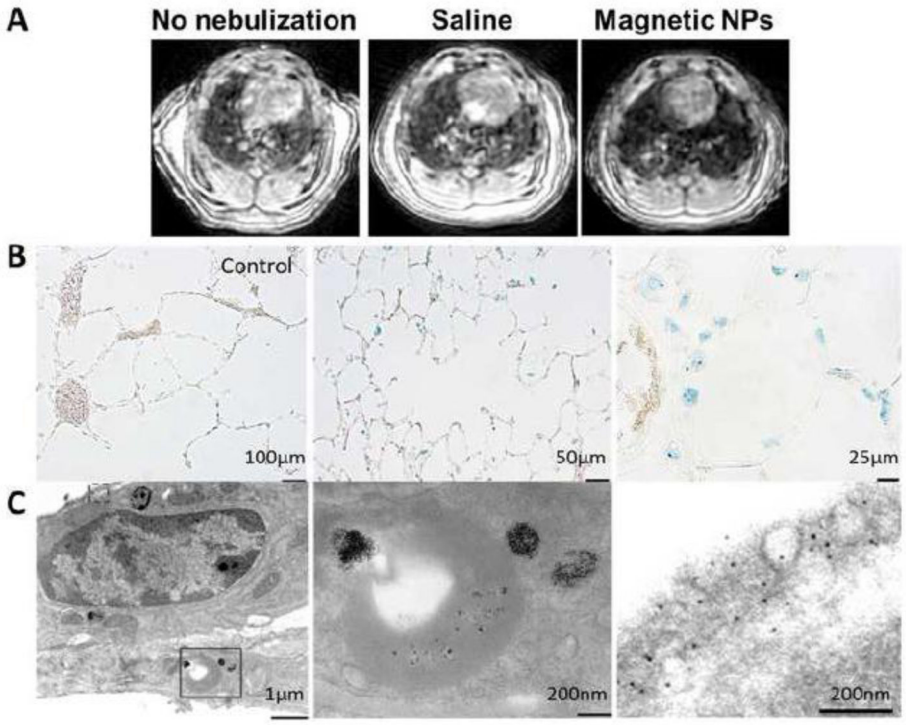

Figure 3.

In vivo distribution of aerosolized SPIO-NPs in rat lung. (**A**) Inhaled magnetic NPs lowers signal intensity of lung parenchyma on UTE MRI consistent with the "negative contrast" effect of iron oxide. Control rats were untreated or received nebulized saline. (**B**) Prussian blue stain for iron following inhalation of saline (*left*, bar=100μm) or SPIO-NPs (*middle*, bar=50μm, *right*, bar=25μm). (**C**) TEM images show degrading SPIO-NPs within alveolar septal cells (*left*, bar=1μm). The solid rectangle inset is shown at a higher magnification (*middle panel*, bar=200nm). The dashed rectangle inset is shown at a still higher magnification to demonstrate free iron oxide particles within alveolar type-1 epithelium (*right panel*, bar=200nm)

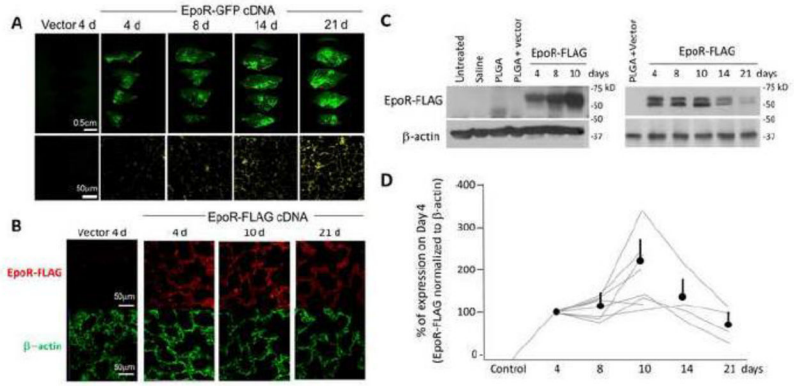

Figure 4.

Inhalation of nebulized PLGA NPs containing either EpoR-GFP cDNA or vector in rat lung. **(A)** *Upper row:* Biofluorescence of serial slices through the right caudal lobe fixed at different times following nebulization (bar=0.5cm). *Lower row:* Representative histological sections of inflation-fixed lung under fluorescent microscopy (bar=50μm). (**B**) Representative immunohistochemistry of cryosectioned lung show expression of EpoR-FLAG, β-actin and DAPI stained nuclei. Bar=50μm. (**C)** Representative immunoblots of EpoR-FLAG expression in the lung. Multiple experiments were performed using independent samples from different locations (2 blots are shown). Initial experiments used multiple negative controls and shorter follow-up (*left*). Later experiment used a single control and longer time course (*right*). Exogenous EpoR-FLAG expression was quantified with anti-FLAG antibody and β-actin (loading control). **(D)** Summary of all immunoblots. FLAG signal on the control samples were all zero, so EpoR-FLAG expression was quantified against expression on Day 4 arbitrarily set as 100%; with Day 4 being a time point common to all experiments. Each line represents one series of experiments where control and experimental samples were loaded on the same gel. All individual trend lines and the average (±SD) expression at each time point were significantly higher than control level (100%) ($p<0.05$).

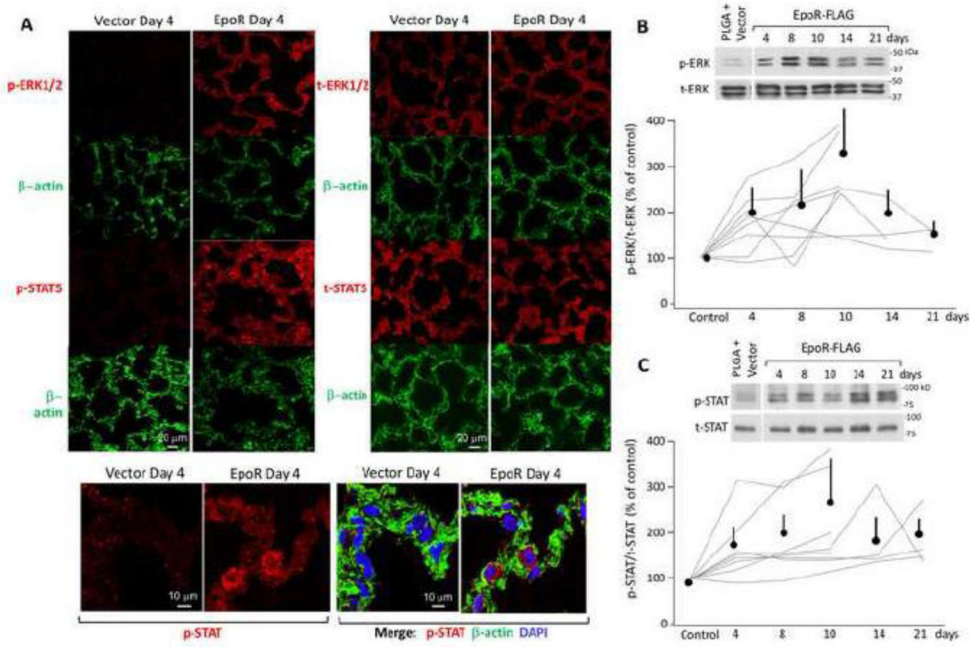

Figure 5.

Activation of EpoR signal transduction in lung tissue following inhalation of aerosolized PLGA NPs containing either EpoR-FLAG cDNA or vector. Lungs were harvested after the indicated number of days. Negative controls were performed with vector-bearing PLGA-NP. Ratio of phospho- (p-) to total (t-) ERK1/2 and STAT5 are shown. (**A**) Representative immunohistochemistry of expression of p-ERK, t-ERK, p-STAT5, t-STAT5, and β-actin. DAPI stained the nuclei. Bar=20μm. (**B**) Representative immunoblot of p-ERK and t-ERK (*top panel*). The p/t-ERK signal ratios were normalized to that in vector-treated lungs, which was set as 100% (*lower panel*). (**C**) Representative immunoblot of p-STAT5 and t-STAT5 (*top panel*). The p/t-STAT signal ratios were normalized to that in vector-treated lungs, which was set as 100% (*lower panel*). In (**B**) and (**C**), all immunoblot experiments are shown. Each line represents one series of experiments where control and experimental samples were loaded on the same gel. All individual trend lines and the average (±SD) expression at each time point were significantly higher than control level (100%) ($p<0.05$).

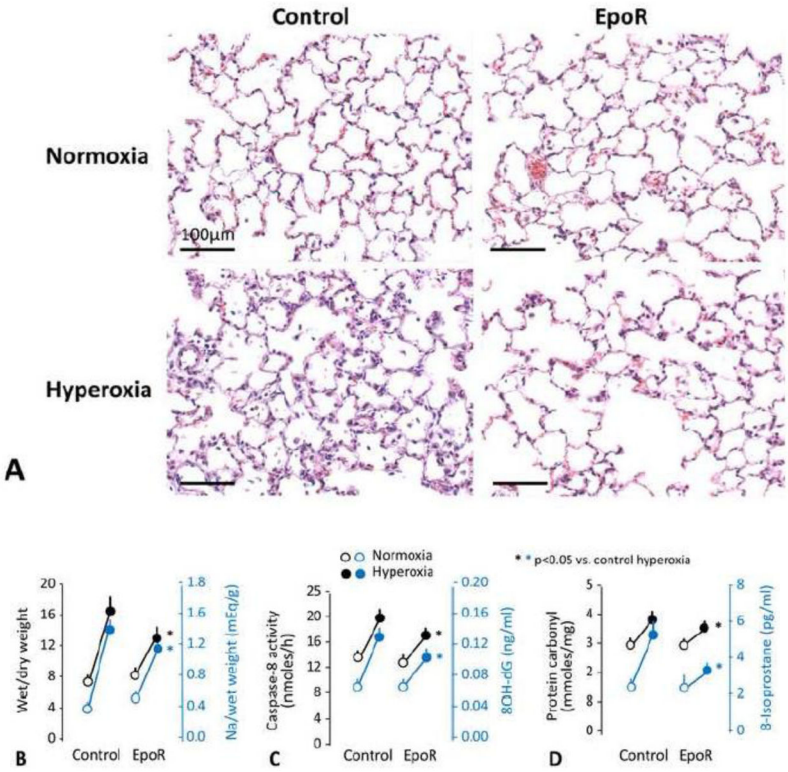

Figure 6.

Effects of EpoR-FLAG cDNA inhalation on oxidant damage in lung tissue. Rats received aerosolized PLGA NPs containing either EpoR-FLAG or vector only, and were exposed to acute hyperoxia one week later, compared to corresponding control animals exposed to normoxia. (**A**) Representative histologic sections of distal lung. Trichrome stain. Bar=100μm. (**B**) Wet/dry (*black*) and sodium (Na)/dry (*blue*) weight ratios. (**C**) Caspase-8 activity (*black*) and oxidative DNA damage measured by 8-hydroxy-2′-deoxyguanosine (8-OHdG) level (*blue*). (**D**) Protein and lipid oxidation measured by carbonyl (*black*) and 8-isoprostane (*blue*) levels, respectively. Mean±SD. All increases from normoxia (open circles) to hyperoxia (closed circles) are significant ($p<0.001$). * $P<0.05$ EpoR cDNA hyperoxia vs. control hyperoxia.

Table 1

Physical properties of different PLGA nanoparticles

Content of Nanoparticles	Size (nm)	Polydispersity	Zeta potential (mV)
SPIO	250 ± 97	0.22±0.01	−38±0.5
Canine EpoR-FLAG cDNA or human EpoR-GFP cDNA	196 ± 36	0.04 ± 0.02	−20.63 ± 0.80
Empty vector	186 ± 44	0.07 ± 0.01	−21.48 ± 2.09

Mean±SD.